Single Crystal Tests of Three Dimensional X-ray Diffraction Microscopy

R.M. Suter,[1], D. Hennessy,[1], C. Xiao,[1], and U. Lienert[2]
[1] *Department of Physics, Carnegie Mellon University, Pittsburgh, PA and*
[2] *Advanced Photon Source, Argonne National Laboratory, Argonne, IL*

Introduction

Three dimensional x-ray diffraction microscopy is an emerging set of techniques for probing structure deep inside bulk materials [1]. The primary aim of the work described here is to obtain complete three dimensional maps of microstructure in polycrystals so that the evolution of internal structure under a variety of stimuli can be studied in real time. We describe developments at the APS for doing these measurements and illustrate results of tests of the technique and analysis using single crystals as calibration samples.

For our purposes, "microstructure" refers to the geometry and orientation of single crystal grains within a material. Thus, we wish to generate maps of crystallographic phase and orientation specified by, say, three Euler angles, as a function of position in three dimensions. To do this, we use high energy x-rays (50keV) that penetrate through millimeters to centimeters of solid materials. The x-rays are focused in the vertical direction with a bent silicon Laue monochromator to a height $< 2\mu$m, while the horizontal extent of the beam can be adjusted with slits from ~ 10 microns to over 1 mm. This beam illuminates a planar section of the sample. Successive sections are obtained by translating the sample about the normal to the beam plane.

Data collection procedures used here are similar to those described elsewhere [1,2]. For a given section, CCD images are obtained as the sample is rotated through an interval $\delta\omega$ about an axis normal to the beam plane. For each interval three images are measured at different sample-to-detector distances, L. Such image sets are collected over a sufficient range of ω to generate multiple Bragg peaks, $\mathbf{G}_{hkl}$, from arbitrarily oriented crystalline grains. Because low order Bragg angles are small with high energy x-rays (~ 6 degree for elemental crystals at 50keV), many families of peaks, $\{h, k, l\}$, are intercepted by a relatively small CCD field of view. With a set of $3N_\omega = 100$ to 300 images, the challenge is to reconstruct the planar section of microstructure that would have generated the observed pattern. A set of planar sections can be put together to form a three dimensional microstructure.

Methods and Materials

Experimental set-up. Measurements are made at XOR-1ID-B. We use an optics set-up similar to that at ID-11 at ESRF [3]. To minimize motion of the beam due to thermal expansion, the bent silicon monochromator, housed in a shielded box, is mounted on the same optical table as the rest of the apparatus. The focal length is about one meter. The downstream elements are tilted at $4.6^o = 2\theta^{50keV}_{Si(111)}$. A conventional Huber 410 is used as the ω rotation [4]; xy-translations are mounted on this table and the sample is held in a drill chuck on the top translation. Fig. 1 shows a mounted sample, the beamblock, and the detector system. The detector uses a Ce layer-doped YAG crystal as a scintillator that is coupled to a liquid nitrogen cooled 1k x 1k CCD camera with adjustable magnification. We currently use a nominal 4 micron pixel resolution. The Ce doping layer must be kept thin enough that beams incident at Bragg angles from normal produce negligible broadening as they transit through the active layer. Data reported here use a 1μm layer although even 5μm layers would produce smearing less than 2μm since the scattering angles are 20 degrees and less; the corresponding increase in signal will decrease acquisition time and improve image analysis in future work.

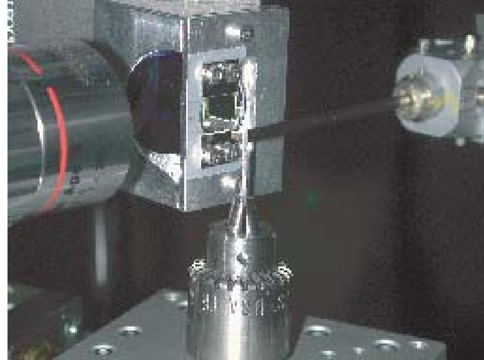

FIG. 1: Sample, beam-block, and detector system. The incident beam enters from the right. The beamblock is a Ta rod with a flat cut at the end. As seen here, the detector system is positioned so that the incident beam is aimed at the bottom of the YAG scintillator. A 45 deg mirror is mounted in the frame that holds the scintillator and the camera lens (left) sees radiation from the mirror.

Samples. We report here on measurements using a single crystal of silicon. The sample is a thinned slice taken from a (111) oriented silicon wafer. The cross-section was $\sim 3 \times 15$mm^2. Additional measurements have been carried out on a $1 \times 1 \times 20$mm^3 aluminum single crystal; these will be briefly discussed. Single crystal measurements serve to validate analysis procedures, pin down experimental parameters, and verify software. They also give a good indication of angular resolution on the Euler angles describing crystal or grain orientations. While they may not be optimal indicators of positional resolution in polycrystal measurements, our analysis does allow some characterization (see below).

Analysis methods. We use a computer program that combines simulation of the measurement physics and geometry with simulation of the sample microstructure. The microstructure and various experimental parameters are adjusted in order to obtain an optimal match of simulated to observed diffraction. We first generate a binary form of the experimental data set. Image analysis steps include median filtering to remove sharp spikes, background subtraction, spot identification, peak intensity determination for each spot and then thresholding at a fraction of the peak height. This binary data set can be processed to remove pixel entries that occur in a large fraction of the images in order to eliminate spurious signals, for example, from the stationary beamstop.

The simulation program creates a grid covering a prescribed planar sample area that can be defined as equal to, larger, or smaller than the sample under study. Each element in the triangular grid is assigned a crystallographic phase and orientation. In the present work, the phase corresponds to either the appropriate crystal structure (phase = 1) or "vac-

uum" (phase = 0) – a region that generates no scattering. The program adjusts the orientation and phase at each grid element to try to match as many observed diffraction peaks as possible. Scattering from each grid element is calculated for each measured interval in ω and is matched against the entire experimental data set. At each ω, element perimeters are "clipped" if necessary at the beam edges so that scattering arises only from the illuminated part of the sample. After adjusting each grid element the entire grid can be refined and another iteration begun. Grid refinement involves dividing each parent triangle into four smaller ones. Only grid elements whose orientation has changed within the previous two iterations (or whose phase is 0) are re-gridded and re-fitted; others are considered to have converged. After all elements have converged or have reached a minimum size, the fitting is considered complete. After each iteration, a Monte Carlo algorithm can be used to vary a set of experimental parameters (beam energy, detector distances, detector orientation, origin coordinates on the detector, etc.) to improve overlap between the current simulated data and the experimental data. Additional details of the fitting procedure will be described in a forthcoming paper [5].

The fact that scattering from each grid element is compared to the entire experimental data set leads to an improved level of noise immunity compared to back projections of individual diffraction spots; we perform a crude test of this idea here. Counting statistics and variations in lineshape with L generate uncertainties in spot shapes. Due to the small scattering angles, geometrical errors along the incident beam (at a particular ω) are amplified by about a factor of ten relative to the transverse direction [1,2]. With the exception of the current silicon data, we typically collect images over two "wedges" whose centers are rotated by 90 degrees; this assures isotropic position resolution in the sample coordinate system. In the current case, geometrical information, while anisotropic, is determined by comparing to thirty or more observed Bragg peaks. The analysis uses a simulated beam that is larger than the actual beam width so that the program has to resolve edges of the illuminated region. These edges are not sharp due to the sample rotation, but edge resolution is gained by requiring each element to match a large number of observed diffraction spots. Resolving edges between phase = 1 and 0 regions is expected to be more difficult than determining grain boundary positions because there is no competing intensity coming from the adjacent sample area and the measurement relies entirely on the lineshape of the scattering from the sample.

Results

Silicon crystal. The incident beam (Fig. 2) was 100μm wide (FWHM), with constant intensity ($< 2\%$ variation) over the central 78μm. A detailed measurement stepping through a single Bragg peak indicates an ω linewidth of 0.06 degrees; this width is expected due to the $\sim 1\%$ energy bandpass of the bent Laue monochromator. The finite resolution implies that occasionally, even for silicon, a Bragg peak may occur on neighboring oscillation images if the Bragg angle lies close to the edge of a $\delta\omega$ interval. For the mapping measurement, data were collected over $-20 \leq \omega \leq 20$ degrees, relative to incidence along the $< 111 >$ direction with $\delta\omega = 1$ degree. About 35 Bragg peaks were observed at at least the L_1 and L_2 detector positions.

Fig. 3a shows an example of detector images of diffraction from the Si(111) wafer along with the diffraction spots generated by the simulation. Note that the observed colored spots are generated by projecting many small grid elements

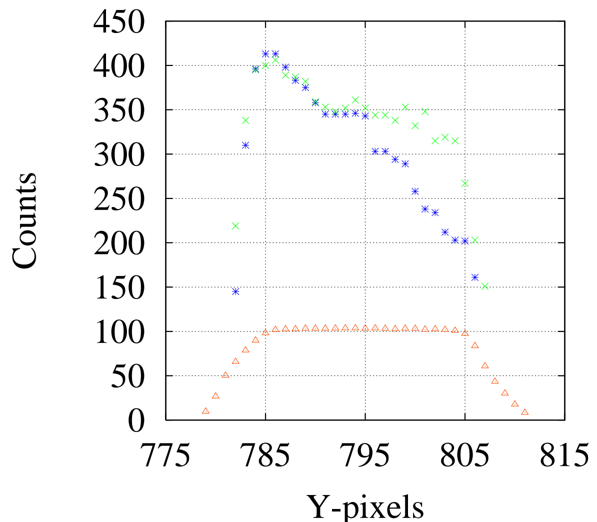

FIG. 2: Measured CCD intensity across a silicon Bragg spot. Blue and green symbols are neighboring horizontal pixel rows at the peak intensity position in the vertical or z direction. Constant intensity contours are slightly tilted relative to the pixel rows due to the finite angle, η (see Fig. 3) for this peak. The red symbols are a cut through the incident beam, shifted and scaled for comparison to the diffraction peaks. The width of the diffracted beam is equal to that of the direct beam. Since the sample is wider than the incident beam, it is the beam that determines the effective "sample size."

along appropriate scattered beam directions. The simulation matches all observed diffracted beams. It also generates additional spots that are not observed in the measurement (one such is seen at the right side of Fig. 3a). These tend to be either low angle (111) peaks that are blocked by the beam block or are at large angles and are apparently too weak to have survived the image analysis processing. The nominal set of Euler angles determined by the simulation is $(350.05, 34.20, 52.85)$ deg with maximum deviations of ± 1.5 deg. However, the deviations are strongly correlated; the crystallographic misorientation angles between grid elements are all within 0.8deg while the standard deviation is 0.2 deg.

Fig. 3(b) shows the 150μm side length simulation grid after fitting. The hexagon is centered on the origin (+ sign in the figure). The fit includes 384 grid elements with side lengths 18.75μm; further refinement is possible and is proceeding [5]. The color code is RGB, with weights based on the Euler angles relative to their full range of $(360, 180, 360)$; thus the red region is that which generates qualifying scattering. This region is surrounded by a white region in which no grid elements produce scattering that overlaps a sufficient number of experimentally observed Bragg peaks. On a much finer color scale, one can see the orientation noise within the scattering region – different grid elements yield different orientations. The simulation is consistent with the measured incident beam size. The sample thickness is determined to be 165μm, consistent with what is known of the thin wafer being measured. The splay of the fitted region on the right side of Fig. 3(b) is presumed to be due to its larger distance from the origin and its correspondingly more rapid motion into and out of the beam as ω is varied.

Aluminum crystal. Here we used a 1.3mm wide incident beam to illuminate essentially an entire cross-section of the

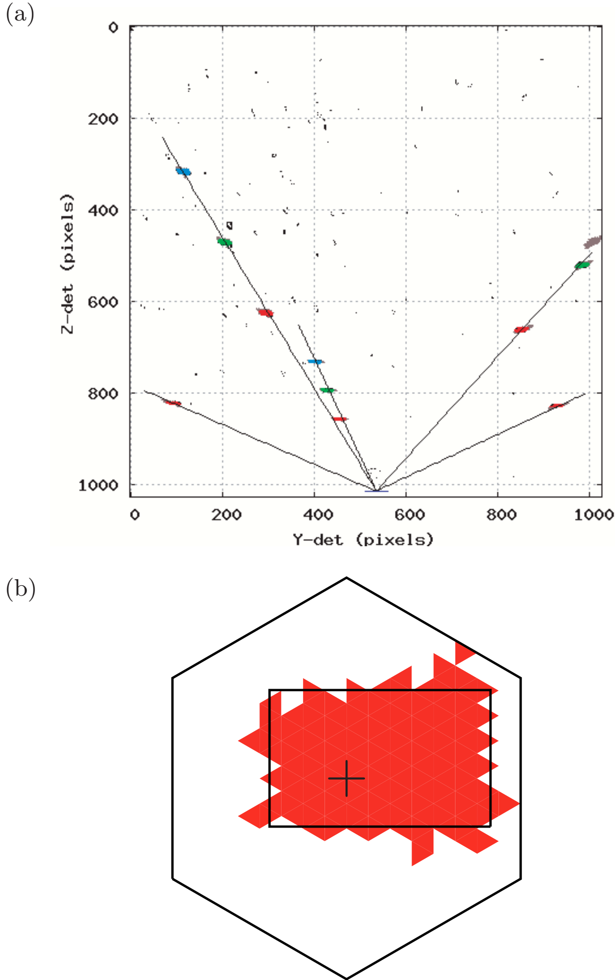

FIG. 3: (a) Superimposed detector images at silicon sample-to-detector distances $L_i = 5.07, 7.07, 9.07$ mm. The beam is incident in the $\hat{x}$ direction, illumination is in the (x, y) plane and $\hat{z}$ is perpendicular to this plane. Experimentally illuminated pixels are shown in black, pixels hit by both the experiment and simulation are in colors (L_1 red, L_2 green, and L_3 blue), while pixels hit by the simulation but not the experiment are brown. The lines emanating from the nominal origin at $(535, 1013)$ are guides to the eye emphasizing the five Bragg peaks observed in this one degree interval of ω (this image is atypical in that most ω intervals contain no Bragg peaks). The angle of these lines measured from vertical is defined as η. Spots at small $|\eta|$ and large scattering angles (second from left solid line, for example) are larger than those near the equator and at small scattering angles due to projection geometry. Due to detector translation imperfections, the three spots do not lie perfectly on the lines (the fitting program corrects for this wobble). The horizontal line centered on the origin represents the size of the simulated incident beam and is twice the width of the beam used in the measurement. (b) Simulation space. The large hexagon (150μm side length) is the gridded sample space plane. The region in red is the fitted geometry of the illuminated region of the silicon single crystal (see text for details). The incident beam travels left-to-right at $\omega = 0$. The height of the rectangular box is 100 microns which is the width of the incident beam. The rectangle length is the deduced thickness of the silicon crystal, $\approx 165\mu$m. The '+' represents the center of rotation deduced by the fit.

sample. Volumetric data covering eight planar sections or slices separated by 50μm were collected before and after annealing the sample at 550C for 30 minutes. The analysis reported here used a 0.5mm side length hexagonal grid. It is clear that significant mosaic structure is present: numerous diffraction spots extend across more than one ω interval. Fits yield simulated diffraction that follows a significant portion of this structure [5] by creating a distribution of grid orientations. Averaging over the eight slices, the average misorientation varies by just over 0.3 degrees before annealing and consistently less than this after annealing. Further work is necessary to make these statements quantitative.

Discussion and Conclusions

We have performed non-destructive studies of the internal microstructure of bulk samples. While these samples have rather simple structure, it is clear that the combination of hardware, data collection procedure, and analysis software used here is sufficient for studies of samples that are more interesting and that it should be possible to follow evolution of microstructure induced by a variety of processes. The orientation resolution is well below one degree even with data collected with $\delta\omega = 1$ degree; smaller integration intervals should lead to even better orientation resolution. Changes in the front end optics should yield improved energy (and therefore angular) resolution. Spatial resolution on the order of 20μm appears to have been achieved. Optimal spatial resolution requires precise knowledge of all experimental parameters. This will be aided by improved hardware including an air bearing rotation stage and detector improvements. Combining silicon calibration data with data on samples of interest should achieve spatial resolution of a few microns. The simulation approach to data analysis can be generalized in a variety of ways: more complex scattering (ex., inclusion of mosaic structure associated with individual grid elements), multiple crystalline phases, and different beam geometries [1].

Acknowledgements

We thank I. Lopez, M. Ubowski, A. Rogers, for assistance in data collection. The XOR-1 staff, including J. Almer, K. Fezza, A. Mashayekhi, R. Ranay, provided valuable and extensive assistance. We have had valuable conversations with H.F. Poulsen. This work was supported primarily by the MRSEC program of the National Science Foundation under Award Number DMR-0079996. Use of the Advanced Photon Source was supported by the U.S. Department of Energy, Office of Science, Office of Basic Energy Sciences, under Contract No. W-31-109-ENG-38.

References

[1] H.F. Poulsen, *Three-Dimensional X-ray Diffraction Microscopy*, Springer Tracts in Modern Physics, Vol 205, G. Höhler, ed., 2004.

[2] E.M. Lauridsen, S. Schmidt, R.M. Suter and H.F. Poulsen, J. Appl. Cryst., **34**, 744–750 (2001) and and H.F. Poulsen, S.F. Nielsen, E.M. Lauridsen, S. Schmidt, R.M. Suter, U. Lienert, L. Margulies, T. Lorentzena and D. Juul Jensen, J. Appl. Cryst., **34**, 751–756 (2001).

[3] U. Lienert, C. Schulze, V. Honkimäki, T. Tschentscher, S. Garbe, O. Hignette, A. Horsewell, M. Lingham, H.F. Poulsen, N.B. Thomsen, E. Ziegler, J. Synch. Rad. **5**, 226-231 (1998).

[4] This rotation stage will soon be replaced by an air bearing precision table with submicron eccentricity.

[5] R.M. Suter, D. Hennessy, C. Xiao, U. Lienert, in preparation.